

Warping prestack imaged data to improve stack quality and resolution

Gabriel Perez¹ and Kurt J. Marfurt²

ABSTRACT

Accurate seismic imaging requires that a geologic feature be located at the same lateral and vertical position in images obtained by 3D prestack migration from different data bins, such as common-offset or common-angle subvolumes. Misalignment of those images degrades the quality of the stack. For dipping reflectors and lateral discontinuities, imperfect imaging causes both lateral and vertical misalignment. In current practice, the vertical component of the misalignment is used to estimate updates in velocity and other imaging parameters; the lateral component is largely ignored. We show that recent developments in seismic-attribute analysis allow us to examine the lateral misalignment of prestack volumes with similar resolution to that achieved in examining vertical moveout. To measure lateral moveout, we pick maxima from local 2D crosscorrelations computed between slices from 3D attribute volumes. We then use these measurements to correct for the lateral misalignment by applying a warping procedure to the corresponding slices in the prestack migrated seismic data. We apply our technique to a 3D land survey acquired over the Fort Worth basin in Texas, and obtain subtle, but potentially important, improvements in the quality and resolution of the stack as well as in the attribute images computed from the corrected data.

INTRODUCTION

The quality of a postmigration stack depends on two related but distinct factors: the individual quality of each prestack trace and the degree of compatibility or similarity between the summed traces. After prestack migration, we expect to see a high degree of similarity between the traces of a common image gather (CIG) because they relate to the same location in the subsurface, although legitimate variations in the signal as a function of offset, angle, or azimuth form the

basis of amplitude variation with offset (AVO) and amplitude variation with angle (AVA) analysis as well as a combination of both (AVOA).

Errors in velocity are a common source of variations between traces, either through inaccurate picking or through incorrect parameterization of the velocity model. The latter might arise from approximating a piecewise constant interval velocity model by an rms velocity model or by approximating an anisotropic medium with an isotropic medium. Whatever the cause, accurate imaging requires that the lateral and vertical (time or depth) location of a geologic feature be the same in every CIG trace, regardless of possible differences in signal character. Misalignment between the images results in a smeared stacked image.

If a reflector is dipping, an incorrect velocity causes not only vertical but also lateral misalignment. Although migration velocity updates lead to lateral and vertical shifts in the position of imaged features, current imaging workflows rely on picking vertical residual moveout of reflectors and commonly do not use lateral misalignment in the image to estimate those updates. This is likely because reflectors in seismic data are less well defined in the lateral direction than in the vertical direction. The development of multitrace volumetric seismic attributes has dramatically increased our ability to image lateral variations sharply in the seismic signal and visualize other geologic features that have lateral expression, such as faults and fracture zones, channel edges, pinch-outs, and unconformities (e.g., Chopra and Marfurt, 2006).

Improving the alignment of imaged data by moveout corrections applied after imaging and before stacking is another way to enhance the quality of the stack. Lateral misalignment of imaged data also contributes to degradation of stack quality. In this article, we present a warping method to correct for horizontal misalignment between prestack migrated images. We rely on the higher lateral resolution of attribute images obtained from the data to measure lateral misalignment.

Lateral moveout corrections change for every image position, and applying those corrections deforms the seismic image. The concept of image registration, or the detection and correction of spatial mis-

Manuscript received by the Editor 1 February 2007; revised manuscript received 18 October 2007; published online 26 January 2008.

¹University of Houston, Allied Geophysics Laboratory, Houston, Texas, U.S.A. E-mail: gpperez@uh.edu.

²Formerly University of Houston, Allied Geophysics Laboratory, Houston, Texas, U.S.A. Presently University of Oklahoma, ConocoPhillips School of Geology and Geophysics, Norman, Oklahoma, U.S.A. E-mail: kmarfurt@ou.edu.

© 2008 Society of Exploration Geophysicists. All rights reserved.

alignment between images, has had considerable attention in the medical imaging and image processing fields, where the deformation process is known as warping (Wolberg, 1990). In seismic imaging, warping has been used for image registration in time-lapse reservoir monitoring (Nickel and Sonneland, 1999; Druzhinin and MacBeth, 2001; Rickett and Lumley, 2001; Hall et al., 2005, 2006; Hall, 2006) and in integrating multicomponent and conventional P-wave data (Fomel et al., 2005). Grubb et al., (2001) assess AVO uncertainties through warping and registering multiple images migrated with different velocity fields. To support the joint registration of P-wave and converted wave data, DeAngelo et al. (2003) identify and interpret geologic features with lateral expression, such as channels and faults, in time slices from coherence attribute images by using an interpretation approach similar to that which we propose.

We begin our discussion by reviewing the basic concepts of image registration and warping. Next, we apply these techniques to identify and correct for lateral moveout in prestack migrated seismic data. We demonstrate the application of prestack warping to improve the quality of the stack by using a 3D seismic data set from the Fort Worth basin in Texas. We use volumetric seismic attributes to help identify and measure lateral moveout and to assess the improvement in the quality of the stack image.

PRESTACK SEISMIC DATA WARPING

A warping operation is the transformation of an image following spatial mapping. Specifically, for 2D images such as time or depth slices from a 3D seismic volume, if $d_{in}(u,v)$ is the input and $d_{out}(x,y)$ is the warped image, the mapping assigns a new position (x,y) in the output image to every position (u,v) in the input. Wolberg (1990) refers to this point-to-point mapping as the warping function.

The warping process consists of two steps (Wolberg, 1990; Rickett, 2000). First, we must determine the warping function; then, we need to resample the image in the output coordinate system determined from this mapping. For our purposes, the warping function is defined at every point in an input 2D seismic data slice from a mea-

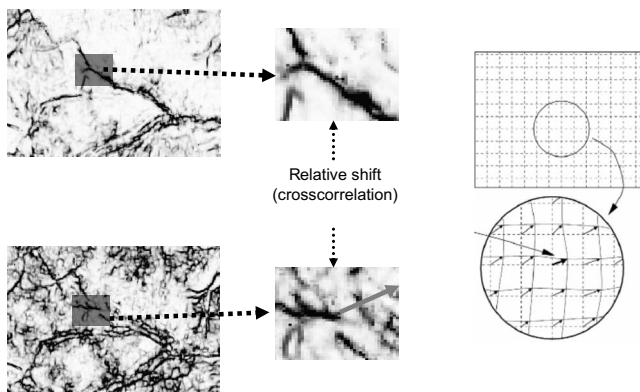


Figure 1. A 2D crosscorrelation between small windows in data from two time slices estimates the local relative misalignment between them. The leftmost panel presents two time slices: input (bottom) and reference (top). The corresponding panels in the center present enlarged versions of the data in two small windows from those slices. The two windows are coincident in size and position. Picking the maximum lag of the 2D crosscorrelation between them provides a shift or misalignment vector, illustrated by the gray arrow in the bottom center panel. Repeating this operation provides misalignment estimates at other positions in the images. Modified from Rickett and Lumley (2001).

surement of the misalignment of the image at that point. The misalignment will thus be corrected for by the warping process. If $[dx(u,v), dy(u,v)]$ is a measurement of the misalignment in each direction, then the warping transformation is given by

$$d_{out}(x,y) = d_{in}[u + dx(u,v), v + dy(u,v)]. \quad (1)$$

Hereafter, we refer to (dx, dy) as the warping shifts; note that for ease of notation, we drop the reference to dependency of those shifts on the position coordinates (u,v) .

Computing the warping shifts requires a reference image, relative to which we measure the misalignment of each individual image. The large amount of data involved in seismic applications demands an automated approach for that measurement. As in other works (Nickel and Sonneland, 1999; Grubb et al., 2001; Rickett and Lumley, 2001; Hall et al., 2005; Hall, 2006), we compute local crosscorrelation functions between each image and the reference image and then pick the crosscorrelation maximum as an initial estimate of the misalignment. Figure 1 illustrates the estimation of the warping function in two data slices by crosscorrelating corresponding windows of data.

For time or depth slices, the crosscorrelation is a 2D function:

$$c(u,v,l_x,l_y) = \sum_{u=-m_x}^{m_x} \sum_{v=-m_y}^{m_y} d_{in}(u,v)d_{ref}(u + l_x,v + l_y), \quad (2)$$

where $c(u,v,l_x,l_y)$ is a discrete crosscorrelation between the input image d_{in} and the reference image d_{ref} , computed over a window of data samples centered on the (u,v) position and for a discrete 2D lag (l_x,l_y) .

The number of samples in the window along each direction, $2m_x + 1$ and $2m_y + 1$, is small compared to the size of the image in the corresponding direction. For every data sample in the input slice, $c(u,v,l_x,l_y)$ becomes a 2D array indexed over integer lags l_x and l_y in a range of values that is also small compared to the size of the image. We then pick the crosscorrelation maximum and estimate the warping function as the lag corresponding to that maximum.

A conventional and straightforward implementation of equation 2 consists of two loops: an outer loop over spatial positions (u,v) and an inner loop over lags (l_x,l_y) . In the inner loop, cross products are computed and summed for all samples in the window. A closer examination of such an implementation reveals that when the correlation windows overlap, many such cross products and sums are repeated for the same lag in computing the crosscorrelation at two spatially close positions. Therefore, this implementation is computationally inefficient and costly.

For efficiency, most of the authors cited earlier first crosscorrelate and pick maxima on a sparse grid of nodes locally and then compute warping shifts at every point in the image by interpolation and optional smoothing. This was also the case for earlier stages of our work (Perez and Marfurt, 2006a), in which we used a conventional implementation of the crosscorrelation computation. In this article, we apply a more efficient implementation that involves switching the order of the loops. For a given lag in the outer loop, common terms are preserved from one spatial position to the next in the inner loop and the computation proceeds recursively. Though developed independently, our implementation is similar to that of Hale (2006), who discusses efficient computation of crosscorrelations in more detail. This implementation allows us to compute a local crosscorrela-

tion and then find a warping function directly from the data for every point in the image. In this way, we improve resolution in our estimate of the warping function and avoid interpolation issues.

Finally, picking the crosscorrelation maxima provides estimates of the warping shifts, which are integer multiples of the spatial sampling interval in the data. We can think of the crosscorrelation as a continuous function that fits the values computed at the discrete locations given by the data sampling but whose absolute maximum lies, in general, at an unsampled location. Finding the location of the absolute maximum provides noninteger estimates of the shifts. In a last step, we achieve such subsampling precision in estimating the shifts, computing the location of the maximum by applying the Newton-Raphson method using the integer-value pick as an initial estimate. Hall (2006) and Hale (2006) use a similar approach.

To correct for lateral residual moveout, every time or depth slice in a given seismic volume is warped independently and only in the horizontal plane (i.e., no vertical shifts), so the crosscorrelations are two-dimensional and the warping function consists of 2D shift vectors. We can think of the warping function thus determined as a discrete realization of an underlying continuous warping transformation that maps from the input to the warped coordinate system. Conceptually, the final warping step places the data in the warped system and then resamples them, typically in a grid with the same spacing as the input image.

Figure 2 illustrates two approaches to implementing a warping operation. In our implementation, we loop over every node on the output grid and find the corresponding position in the input coordinate system. If, as before, we denote the output node position by (x, y) , the mapping implemented is thus

$$d_{\text{out}}(x, y) = d_{\text{in}}[u(x, y), v(x, y)], \quad (3)$$

where we can think of $[u(x, y), v(x, y)] = [x + dx'(x, y), y + dy'(x, y)]$ as the original location of the node, prior to the warping transformation. The mapping in equation 3 operates from the warped to the input coordinate system (see Figure 2b). The order is reversed relative to the mapping defined in equation 1, so this is the inverse of the warping transformation (Wolberg, 1990). In our application, establishing this inverse mapping requires reversing the order of the terms in the crosscorrelation and picking discussed above. Also, the notation $[dx'(x, y), dy'(x, y)]$ highlights the conceptual difference between the warping shifts here and those in the previous discussion.

As described, warping is a computationally efficient collection of point-by-point operations. In general, the discrete realization of inverse mapping provides a position $[u(x, y), v(x, y)]$ in the input coordinate system that does not necessarily match a location in the input sampling grid (see Figure 2b). To implement the mapping in equation 3, we must use interpolation to estimate a data value $d_{\text{in}}[u(x, y), v(x, y)]$ at the unsampled position. Our preferred interpolation method is local and is limited to the four data values derived by inverse mapping that are closest to the interpolation location; we use simple bilinear interpolation. Short, local interpolation operators conform to the relatively rough character of the data (some volumetric seismic attribute images are particularly rough) when examined in time or depth slices and specifically avoid smearing the image across faults and other discontinuities.

For application to 3D prestack imaged data, we independently warp every one of the data subvolumes derived by sorting the data (typically binning by offset, angle, or azimuth). For every subvolume, warping is implemented slice by slice, and the warped slices are reassembled into a warped version of the volume. As a reference

for the crosscorrelation, we typically use the current version of the stack; another possible choice for reference would be a short-offset or short-angle partial stack. Figures 1 and 3 illustrate the process for an individual slice, resulting in the warped slice at the bottom of Figure 3. Finally, we merge all of the warped subvolumes, sort them into CIGs, and stack them.

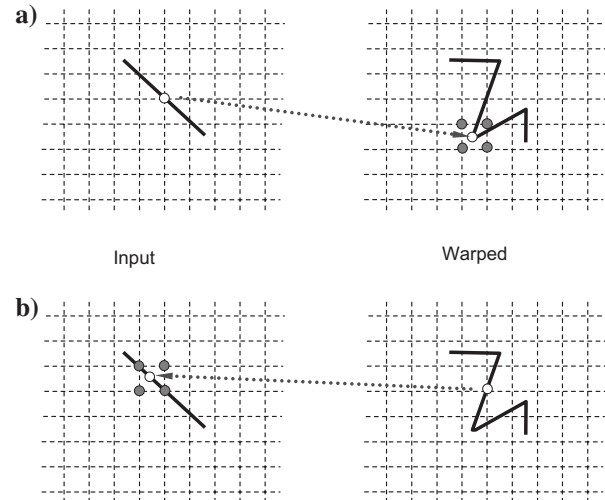


Figure 2. Two possible warping implementations: (a) looping over positions in the input image and (b) looping over positions in the output or warped image. Solid black lines show a corresponding feature in the input image and the warped image. In (a), the white dot marks a position in the discrete grid of the input image as well as the corresponding position in the warped image determined by mapping from the input to the warped image, as indicated by the gray dotted arrow. The warped position does not in general map onto a sampling grid point. Construction of the warped image proceeds by estimating the unknown values at grid points (gray dots) by interpolating from the known but irregularly sampled values at the warped positions. This can be a computationally complex operation. In (b), the white dot marks a position in the grid in the output image, and the gray dotted arrow shows the corresponding location in the input grid. Note that the direction of the arrow is reversed, indicating the mapping in (a) and (b) are inverse to each other. The white dot in (b) does not in general fall on a grid point, but simple point-by-point interpolation from the known and regularly sampled input values (gray dots) provides an image value at the desired output position.

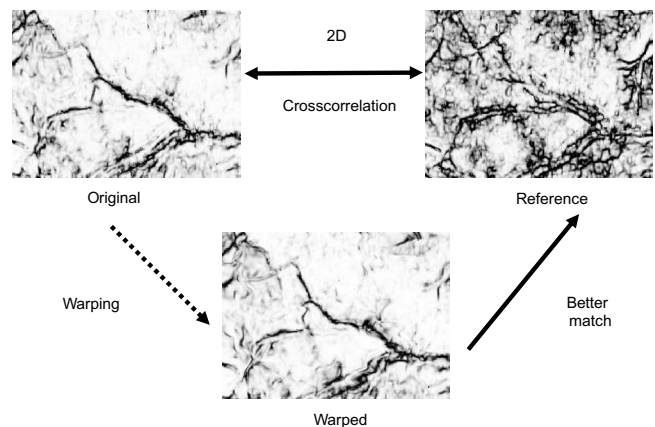


Figure 3. Shifts computed from the 2D crosscorrelation can be used to distort the slice data in a space-variant way so that the alignment of individual features of the warped image better matches those of the reference.

We prefer to estimate our warp function from selected attribute images obtained from individual seismic volumes rather than from the conventional seismic data. We choose volumetric seismic attributes that enhance the appearance of discrete lateral discontinuities and flexures and eliminate detailed sensitivity to the seismic wavelet. We also choose the attribute volume computed from the stack as a reference in the crosscorrelation and shift estimation process. We compare images from the warped stack volume to corresponding images in the input stack as a means to assess the performance of the warping process. To assist in this assessment, we also compute attributes from the warped data and compare them to the attributes computed from the input data. Figure 4 summarizes the processing flow.

APPLICATION TO FIELD DATA

We applied the processing flow of Figure 4 to a land data set from the Fort Worth basin. The data available to us consisted of preprocessed (i.e., with statics and noise attenuation applied) common-midpoint (CMP) gathers. We migrated the data with a prestack time-migration process that outputs the imaged data into common-angle bins; in this case, we binned the output in the 0° – 65° range, with 1° spacing between bins.

Angle binning allows for a simple and very effective correction for wavelet stretch that increases the effective fold and quality of the stack and the resolution of large-angle imaged data (see Perez and Marfurt, 2006b, 2007). The correction for stretch involves applying a spectral shaping operator that balances the spectral content of the migrated data across angles, relative to a partial stack in a narrow range of near-zero angles. If present, differences in spectral character in the data can negatively influence the accuracy in estimating warping shifts, as discussed by Fomel et al. (2005). For this reason,

correction for stretch also suitably conditions the data for the warping process. Applying spectral matching operators is also a preprocessing step in time-lapse applications. Although the main purpose is to compute meaningful differences, spectral shaping also helps to improve the warping process (Druzhinin and MacBeth, 2001; Rickett and Lumley, 2001; Hall et al., 2005, 2006; Hall, 2006). Our migration process also included a data-dependent vertical residual moveout correction, so that little or no vertical (i.e., time) misalignment was present across angles in the migrated CIGs before warping was applied.

We computed coherence and curvature attributes (e.g., Chopra and Marfurt, 2006) for the postmigration stack and for each of the common-angle subvolumes before performing several warping procedures. To find the warping shifts, in each of those procedures we crosscorrelated data from each of the attribute subvolumes (i.e., the individual angle bins) with the corresponding attribute volume from the stack. We also computed the warping function by crosscorrelating the migrated data rather than an attribute volume. Best results came from using the most negative curvature attribute to estimate the warping function. As opposed to coherence attributes, computation of curvature attributes involves long operators and provides an image of long-wavelength structural features (Chopra and Marfurt, 2006). For this data set, the curvature operator length was roughly 30 times the trace spacing, or about 1 km. In other work in this area, curvature has been very useful in picking fracture systems, faults, and joints with little or no displacement (Hakami et al., 2004; Blumentritt et al., 2006).

Figure 5 illustrates the estimation of the warping shifts for the slice at $t = 1.36$ s. Even after prestack migration, the image from seismic data in the individual bins is noisy and poorly resolved compared to the stack. A similar comparison between the stack and each individual bin for the attribute data reveals the attribute image from the stack is still better quality, but the differences with the attribute images from individual bins are not as marked as with the regular seismic data.

The most negative curvature images in Figure 5c and d highlight major geologic features, such as the two southwest-northeast-trending faults and a system of less pronounced lineaments that run parallel and perpendicular to them. In a time slice from the regular seismic data, we also have lateral variations that reflect geologic structure cutting the time slice; at some places, the slice cuts a peak and at others it cuts a trough, even though there is no discontinuity. Because the effect of the seismic wavelet has been removed in the curvature computation, the lineaments we see are geological or they represent noise. The long-wavelength operator in the curvature computation removes noise. Therefore, it is more fruitful to measure local misalignment by crosscorrelation between the relatively isolated and distinct features in the curvature images than between the smoother and noisier images from the regular seismic data.

We computed crosscorrelations on local windows for all points in the images, such as those in Figure 5c and d. We used a square crosscorrelation window with 21 traces (2200 ft, 670 m) on each side and allowed a maximum crosscorrela-

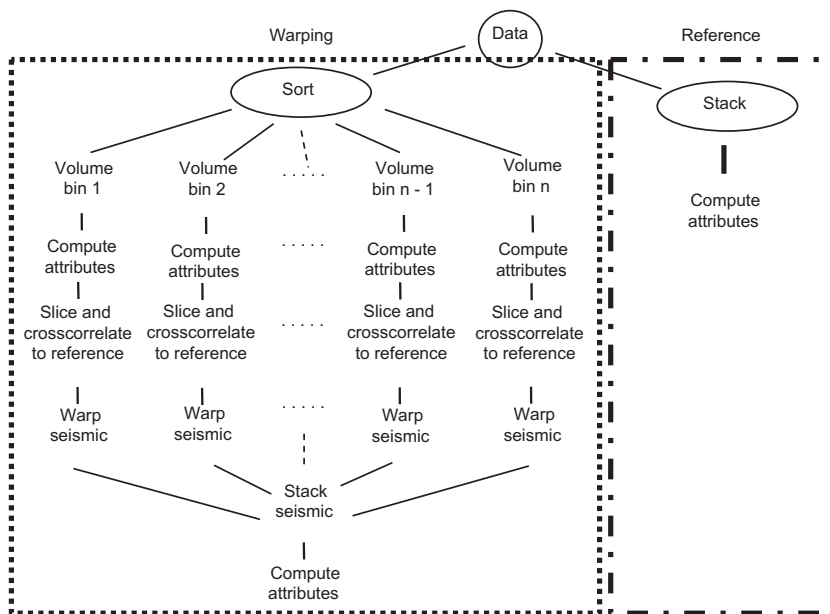


Figure 4. Processing flow to warp and then stack data from individual bin subvolumes. The warping function can be computed by crosscorrelation between slices of seismic data or between slices of attribute data. For the former, the reference is taken from the stack volume; for the latter, the reference is taken from an attribute volume computed for the stack. In all cases, the warping function is applied to the original seismic data.

tion shift of eight traces (880 ft, 270 m) both inline and crossline. Shifts from crosscorrelations in Figure 5e and f are rough in character and are presumably biased by noise. Even though significant shifts follow many of the features from the curvature images, large shift values are also present in some areas where noise dominates and there are no significant features.

The seismic data slices to which warping is applied are generally smooth. Therefore, the warping shifts should also be smooth; large or abrupt local variations in the warping shifts result in undesirably jagged or locally distorted warped images (Wolberg, 1990; Rickett and Lumley, 2001). On the other hand, the maximum crosscorrelation values are good indicators of the signal content of the data (Figure 5g); large crosscorrelation values align along the location of the major and most significant geologic features, and low values highlight zones with poor or no signal. We suggest that besides being smooth, the magnitude of the warping shifts should also be governed by the most significant geologic features. Specifically, in an area with low values of the maximum crosscorrelation coefficient, that magnitude should be similar to the values of raw crosscorrelation shifts computed for nearby areas with high values of the maximum crosscorrelation, regardless of the local value of those raw shifts. If we visualize the warping as a motion in the image, shifts from the areas of high crosscorrelation pull the image, and areas with little or no signal are passively dragged. A similar concept is presented by Hall (2006) and implemented by modeling the warping as the deformation of a mesh of particles connected by springs.

Our implementation is much simpler. As suggested, we used the magnitude of the maximum crosscorrelation as an indicator of the relative significance of the raw shift values. Thus, we produced final estimates of the warping shifts (Figure 5h and i) as weighted averages of the raw crosscorrelation shifts, using as weights the corresponding maximum crosscorrelation values, on square windows with 21 traces on each side. To preserve vector fidelity, we average the magnitude and direction of shift vectors computed at every position from the (dx, dy) components and then compute new values of those components from the average magnitude and direction. The size of the window matches our rough estimate of the average separation between major geologic features in the slices from the curvature attribute data. As desired, the final shift values are smooth. Because of the weighting choice, they also honor those features with the largest crosscorrelation coefficients.

Figures 6 and 7 illustrate the impact of warping on the quality of the stack and show that warping results in an overall improvement in the signal-to-noise ratio (S/N) of the stack and a sharper image of the southwest-northeast faults. There are subtle, but potentially very important, improvements in the definition and alignment of these faults in the warped stack. Faults are sharpened without exception by warping (Figures 6 and 7). Warping attenuates most of the steeply dipping noise leaking through the shallower times in the original stack (Figure 7). On the other hand, minor deterioration in quality is visible at the edges of the warped image. Warping also results in improved imaging of the large curvature features in the most negative curvature images (Figure 8). Finally, after warping, the overall coherence of the stack increases as a result of improving the quality and S/N of the stack (Figure 9).

DISCUSSION

Moveout is at least a 3D vector with lateral and vertical components; however, the lateral and vertical components cannot be measured with similar precision in a single data set. Compared to vertical moveout, conventional seismic data provide relatively poor defini-

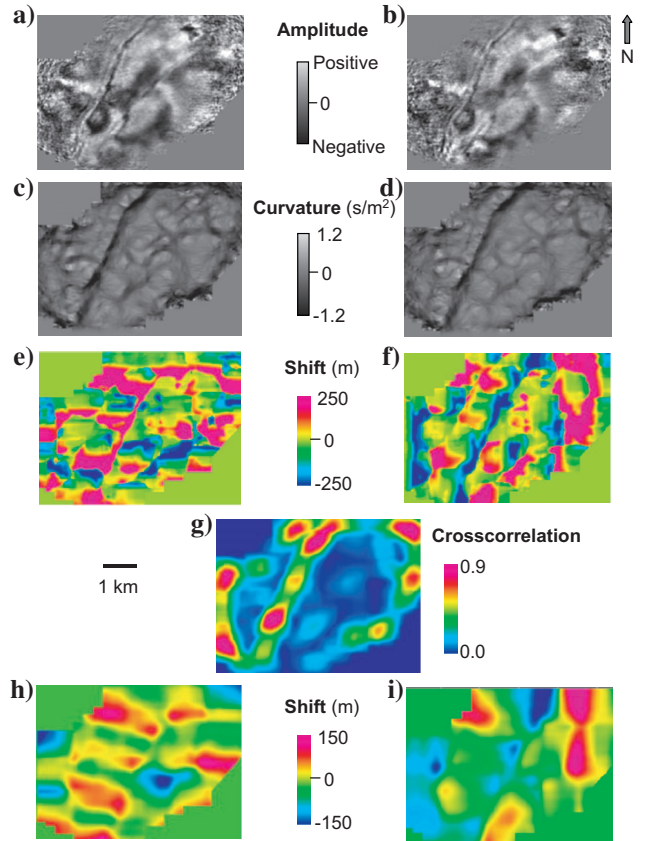


Figure 5. Estimation of warping shifts for a time slice at $t = 1.36$ s. Time slices from (a) the stack volume, (b) the 20° bin subvolume, (c) the most negative curvature volume computed from the stack, and (d) the most negative curvature for the 20° bin. Raw shifts (e) in the inline (east-west) direction, computed by crosscorrelating between (c) and (d), and (f) in the crossline (north-south) direction. (g) Maximum value of the crosscorrelation. Final shifts (h) in the inline direction, computed by crosscorrelation-weighted averaging, and (i) in the crossline direction.

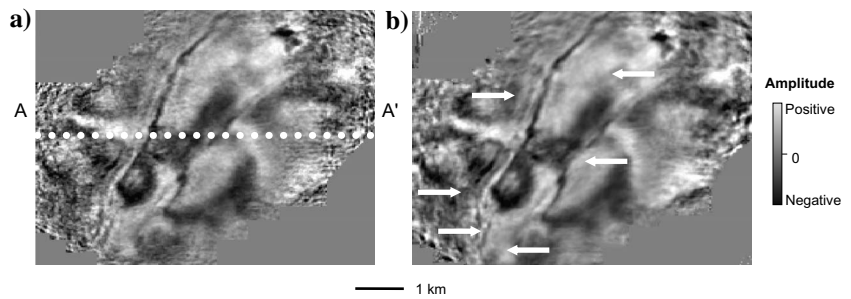


Figure 6. Comparison of time slices at $t = 1.36$ s before and after warping. (a) Original stack, (b) stack after warping. The warped image is less noisy and more sharply resolves the southwest-northeast faults. Arrows point to specific locations where the image is improved by warping. The dotted line in the left image shows the location of the inline of Figure 7.

tion of lateral moveout. This is probably why lateral moveout is not included in current imaging workflows. We use volumetric seismic attributes as a source of lateral moveout measurements because of the increased lateral resolution and definition they provide.

As an alternative to the cascaded vertical residual moveout correction followed by lateral warping presented in this article, we could consider implementing a 3D correction for the full residual moveout vector. However, independent estimation of vertical and horizontal moveout on different data sets will result in quantities that are, in principle, decoupled. In other words, the ideal 3D vector will differ from the vector assembled from those independent measurements. Our cascaded approach provides a robust way to avoid these issues; it should work as long as vertical moveout is dominant and lateral moveout is relatively small. Although further quantification is

needed, it seems reasonable to expect that this is true where dip is low to moderate. If lateral moveout is large, then the order of the steps can be switched in the cascade application.

It is also important to note that seismic images binned by subsurface parameters such as reflection angle are coupled across bins because those parameters are estimated as part of the migration. For instance, velocity errors translate as errors in the angle estimation, so the image is shifted across angles. Thus, residual moveout becomes a 4D vector — even 5D if subsurface azimuth is included in the binning. Our cascaded and simplified approach is all the more justified in our case study because dip is low and vertical moveout is dominant. If residual moveout is large in both horizontal and vertical directions or if there are conflicting dips, a simple point-to-point warp

will likely not properly correct for the residual moveout. A residual convolutional migration operator will be needed.

Computing crosscorrelations and picking maxima at every data point, instead of on a sparse grid, provides strength and robustness to our warping implementation. Besides avoiding interpolation issues, the fine sampling allowed by efficient computation of crosscorrelations provides good resolution in all stages of the shift estimation and analysis process. However, there is a trade-off in resolution versus stability and robustness of the computation, and it is related to the size of the crosscorrelation window. The larger that size, the more stable and less resolved the raw shifts will be. A further limitation in resolution arises from the estimation of a smooth set of warping shifts, in turn related to the size of the window in the crosscorrelation weighted averaging. As noted above, in the application presented here, the size of those windows is consistent with a rough estimate of the expected dominant wavelength of the warping shifts.

In relation to his work with poststack data, Rickett (2000) singles out the presence of noise and the related occurrence of cycle skipping in the crosscorrelation as a major issue for the robust and accurate estimate of shifts in the warping function. It is even more problematic in our application dealing with prestack data. In the first place, we relied on applying common noise-attenuation procedures (e.g., $f-k$ filtering, $f-x$ deconvolution, or other multichannel filtering) to the prestack migrated data. As noted earlier (see “Application to field data”), relative to the stack, prestack attribute images are less noisy than the corresponding prestack images from conventional seismic data. The reduction in noise content is a convenient side benefit of using attribute data for warping estimates. Finally, the crosscorrelation weighted average provides an additional reduction of noise in the raw shifts.

To further constrain and stabilize the shift computation, we could invoke consistency in the variation of shifts across different bins to support filtering and smoothing the raw shifts in that domain. We could also enforce consistency across

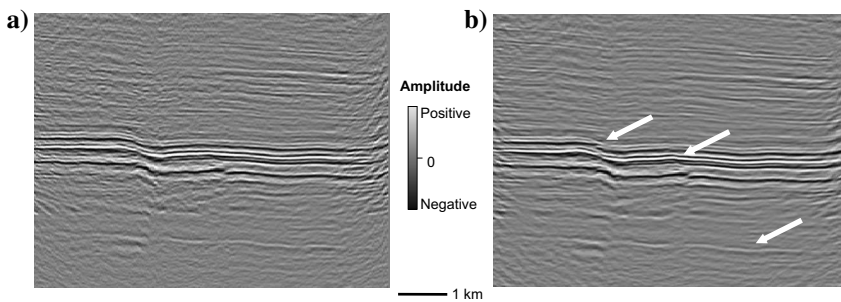


Figure 7. Comparison images for inline AA'. (a) Original stack, (b) stack after warping. Arrows point to specific locations where the image is improved by warping. The location of inline AA' is shown in Figure 6.

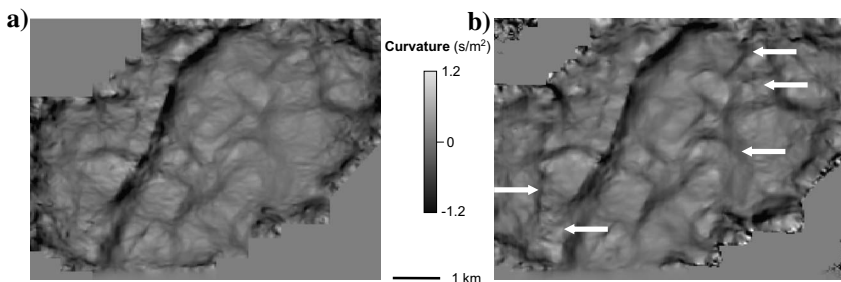


Figure 8. Comparison before and after warping time slices at $t = 1.36$ s from the most negative curvature volumes. (a) Original stack, (b) stack after warping. Arrows point to specific locations where the image is improved by warping.

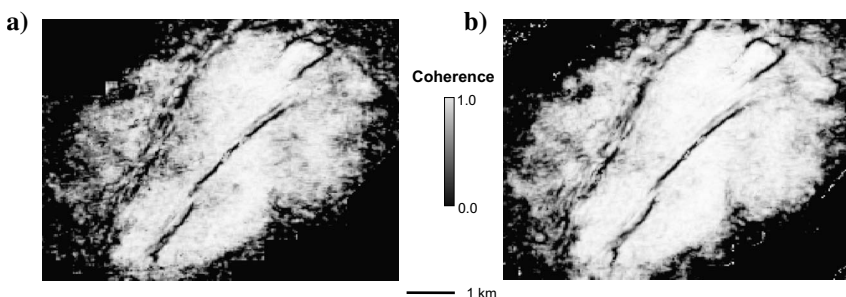


Figure 9. Comparison before and after warping time slices at $t = 1.36$ s from coherence volumes. (a) Original stack, (b) stack after warping. Coherence is increased after warping, indicating a better stack.

bins by crosscorrelation between data from neighboring bins. This procedure computes bin-to-bin incremental shifts; summation of the incremental shifts in an integration computation provides cumulative shifts to the reference. As an added benefit, this alternative helps address the presence of large differences in spectral character and content in the data across bins and relative to the stack, as suggested by Perez and Marfurt (2006a).

As discussed, the correction for stretch in angle-binned migrated data provides our preferred way of dealing with the issue of spectral differences in the data. For other binning, we note that major factors influencing spectral differences, such as attenuation, spherical spreading, and migration stretch, are predominantly time variant. Therefore, if lateral variation in spectral character (i.e., at constant time or depth) is small, we would expect that the spectral differences could be treated approximately by balancing operators that are constant over a given time or depth slice.

Other suggested applications for our work include the use of warping shifts as input to tomographic estimation of velocity updates or as a diagnostic of quality and associated risk in an imaging project.

CONCLUSIONS

The development of volumetric seismic attributes and associated interpretation workflows currently allows us to measure lateral misalignment in 3D-imaged data prior to stack. We have introduced an automated warping procedure to measure and correct lateral misalignments and thus improve the quality and resolution of the stacked image. Our method is applied to uninterpreted time slices and, because it does not rely on the presence or definition of reflectors, it is applicable in areas of complex geology or in other situations where interpretation of reflectors is difficult. On the other hand, the method performs better in the presence of geologic features with a lateral expression, such as faults and fracture zones, channel edges, pinch-outs, and unconformities. Preprocessing the data to mitigate possible spectral differences between data bins is a prerequisite for applying the warping process. As a side benefit, the spectral balancing might also attenuate some of the noise commonly present in prestack data.

We envision that a new generation of tomography algorithms can take advantage of full-vector moveout information to determine better constrained and more accurate velocity models. At the very least, interpretation of 3D residual moveout information can provide insight into the quality and risk associated with particular imaging projects and can also help determine whether factors such as lateral velocity variation or anisotropy are treated properly.

ACKNOWLEDGMENTS

We thank the sponsors of Allied Geophysical Laboratories and the Petroleum Research Fund (American Chemical Society) for their support, and Devon Energy for permission to use their data.

REFERENCES

- Blumentritt, C. H., K. J. Marfurt, and E. C. Sullivan, 2006, Volume-based curvature computations illuminate fracture orientations — Early to mid-Paleozoic, Central basin platform, West Texas: *Geophysics*, **71**, no. 5, B159–B166.
- Chopra, S., and K. J. Marfurt, 2006, Seismic attributes for prospect identification and reservoir characterization, SEG.
- DeAngelo, M. V., M. Backus, B. Hardage, P. Murray, and S. Knapp, 2003, Depth registration of P-wave and C-wave seismic data for shallow marine sediment characterization, Gulf of Mexico: *The Leading Edge*, **22**, 96–105.
- Druzhinin, A., and C. MacBeth, 2001, Robust cross-equalization of 4D-4C PZ migrated data at Teal South: 71st Annual International Meeting, SEG, Expanded Abstracts, 1670–1673.
- Fomel, S., M. Backus, K. Fouad., B. Hardage, and G. Winters, 2005, A multi-step approach to multicomponent seismic image registration with application to a West Texas carbonate reservoir study: 75th Annual International Meeting, SEG, Expanded Abstracts, 1018–1021.
- Grubb, H., A. Tura, and C. Hanitzsch, 2001, Estimating and interpreting velocity uncertainty in migrated images and AVO attributes: *Geophysics*, **66**, 1208–1216.
- Hakami, A., K. J. Marfurt, and S. al-Dossary, 2004, Curvature attribute and seismic interpretation, Case study from Fort Worth basin, Texas, U.S.: 74th Annual International Meeting, SEG, Expanded Abstracts, 544–547.
- Hale, D., 2006, Fast local cross-correlations of images: 76th Annual International Meeting, SEG, Expanded Abstracts, 3160–3163.
- Hall, S. A., 2006, A methodology for 7D warping and deformation monitoring using time-lapse seismic data: *Geophysics*, **71**, no. 1, O21–O31.
- Hall, S. A., C. MacBeth, O. Barkved, and P. Wild, 2005, Cross-matching with interpreted warping of 3D streamer and 3D ocean-bottom-cable data at Valhall for time-lapse assessment: *Geophysical Prospecting*, **53**, 283–297.
- Hall, S. A., C. MacBeth, J. Stammeijer, and M. Omerod, 2006, Time-lapse seismic analysis of pressure depletion in the Southern gas basin: *Geophysical Prospecting*, **54**, 63–73.
- Nickel, M., and L. Sonneland, 1999, Non-rigid matching of migrated time-lapse seismic: 69th Annual International Meeting, SEG, Expanded Abstracts, 872–875.
- Perez, G., and K. J. Marfurt, 2006a, Fine-tuning your seismic image, Prestack data warping to improve stack quality and resolution: 76th Annual International Meeting, SEG, Expanded Abstracts, 2475–2478.
- , 2006b, Correcting for wavelet stretch in common-angle migration improves vertical and lateral resolution: 76th Annual International Meeting, SEG, Expanded Abstracts, 254–258.
- , 2007, Improving lateral and vertical resolution of seismic images by correcting for wavelet stretch in common-angle migration: *Geophysics*, **72**, no. 6, C95–C104.
- Rickett, J., 2000, Data alignment with non-stationary shaping filters: Stanford Exploration Project report SEP 103, 205–215.
- Rickett, J., and D. E. Lumley, 2001, Cross-equalization data processing for time-lapse seismic reservoir monitoring: A case study from the Gulf of Mexico: *Geophysics*, **66**, 1015–1025.
- Wolberg, G., 1990, *Digital image warping*: IEEE Computer Society Press.